Biophysical Journal, Volume 99

Supporting Material

Modeling smooth muscle myosin's two heads: long-lived enzymatic roles and phosphorylation-dependent equilibria

Sam Walcott and David M. Warshaw

Supplementary material for modeling smooth muscle myosin's two heads: long-lived enzymatic roles and phosphorylation-dependent equilibria

Sam Walcott[1]
Mechanical Engineering,
Johns Hopkins University, Baltimore, MD

David M. Warshaw
Molecular Physiology and Biophysics,
University of Vermont, Burlington, VT

[1]Corresponding author. Address: Mechanical Engineering, Johns Hopkins University, 223 Latrobe Hall, 3400 N. Charles St., Baltimore, MD 21218, U.S.A., Tel.: (000)000-0000, Fax: (000)000-0000

Here we present detailed calculations to back up claims made in the text. We start with a table of contents and a glossary of symbols, so that the reader can quickly find a section referred to in the text and comprehend all of the mathematical symbols therein. Note that the derivations assume that the reader has a level of mathematical sophistication that is not assumed in the main text.

Table of Contents

Glossary

Variable	Definition
2P	Myosin with both light chains phosphorylated
1P	Myosin with one light chains phosphorylated
0P	Myosin with neither light chains phosphorylated
HMM	Heavy meromyosin, a double-headed fragment of myosin
$\boldsymbol{n}$	General state vector, whose i^{th} entry (n_i) is the probability that a molecule is in state i
$\boldsymbol{A}$	General rate constant matrix, relating the vector $\boldsymbol{n}$ to its time rate of change
S	The number of states in a generic model
$\boldsymbol{A}_{to}$	Rate constant matrix for single ATP turnover experiments
$\boldsymbol{S}$	Eigenvector matrix of $\boldsymbol{A}_{to}$
$\boldsymbol{\Lambda}$	Eigenvalue matrix of $\boldsymbol{A}_{to}$
λ_i	The i^{th} eigenvalue of $\boldsymbol{A}_{to}$
A_i	The amplitude of the i^{th} exponential in the simulated $F(t)$
$\boldsymbol{f}$	Relative fluorescence vector, the i^{th} entry gives the relative fluorescence of state i
F	Relative fluorescence signal from the single turnover experiments
$\boldsymbol{A}_{ss}$	Rate constant matrix for steady-state ATP turnover experiments
V_{ATP}	Steady-state rate of ATP turnover (both generally and for the 2P model)
V_{ATP}^{1P}	Steady-state rate of ATP turnover for the 1P model
$\boldsymbol{k}$	ATP hydrolysis rate vector, the i^{th} entry gives the steady-state ATPase rate of state i
$\boldsymbol{p}$	Generic vector of parameters for a kinetic model
$\boldsymbol{p}^*$	Generic vector of parameters for a kinetic model that optimizes the fit to generic data
k_x	One of a variety of rate constants (e.g. k_s) defined in various figures.
K_m	A constant, defined as $K_m = (k_T + k_d)/k_a$ (see manuscript Fig. 2 for rate constant definitions)
σ	Standard deviation
Δ_{95}	95% confidence interval
Δ_{99}	99% confidence interval
a_1	A constant, defined as $a_1 = 1/(1 + k_2/k_3)$ (see Fig. 4 of text for rate constant definitions)
a_2	A constant, defined as $a_1 = 1/(1 + k_2'/k_3')$ (see Fig. 4)
k_a^{eff}	Effective attachment rate for the 1P model, $k_a^{eff} = a_1 k_a + (1 - a_1)k_a^*$ (see Fig. 4)
k_d^{eff}	Effective detachment rate for the 1P model, $k_d^{eff} = a_2 k_d + (1 - a_2)k_d^*$ (see Fig. 4)
K_m^{1P}	A constant, defined as $K_m = (a_2 k_T + k_d^{eff})/k_a^{eff}$ (see Fig. 4)
r_1, r_2	Switching rates for the actin-associated model
V_{max}	The maximum value of V_{ATP}
K_M	Michaelis-Menten constant from a fit to steady-state ATPase (roughly equivalent to K_m)
n_{ind}	Probability the actin-independent state in a simple model (see Fig. 7)
n_{act}	Probability the actin-dependent state in a simple model (see Fig. 7)
N_h	The total number of myosin heads in the simple model (see Fig. 7)
ℓ_i	One of two rates of a double exponential fit to $F(t)$ for the 2P model
$\mathcal{A}_i$	One of two amplitudes of a double exponential fit to $F(t)$ for the 2P model
ℓ_i^{1P}	One of two rates of a double exponential fit to $F(t)$ for the 1P model
$\mathcal{A}_i^{1P}$	One of two amplitudes of a double exponential fit to $F(t)$ for the 1P model
$\boldsymbol{A}_{to}^{ad}$	Rate constant matrix for heads in the actin-dependent role
F_{ad}	Fluorescence contribution from heads in the actin-dependent role
$\boldsymbol{A}_{to}^{nb}$	Rate constant matrix for heads in the non-/weak-binding role
F_{nb}	Fluorescence contribution from heads in the non-/weak-binding role
D	mean squared difference between $F(t)$ and double exponential fit
N	number of points sampled in $F(t)$
Δt	time between fluorescence sampling in $F(t)$ measurements
T	overall time of fluorescence sampling

1 A 2P model with role-switching during weak binding

In the main text, we assume that the two heads of myosin are fixed in their roles once one of the heads is weakly interacting with actin. Here, we consider the case where the heads may switch roles when weakly bound to actin (see Fig 1).

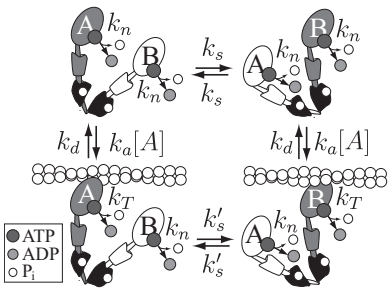

Figure 1: The model for doubly phosphorylated (2P) myosin with role switching during weak-binding. Each head is labeled "A" or "B." The darker head adopts an actin-dependent role and, after binding to actin, may hydrolyze ATP through the actin-dependent pathway (k_T); the lighter head adopts a non-/weak-binding role, and must hydrolyze ATP at its basal rate (k_n). The heads switch roles while unbound with rate k_s, and while weakly bound with rate k'_s. Here, we show that assuming $k'_s = 0$ has little effect on the results of the model.

In this model, which we call the "alternative" 2P model, we consider the general kinetic scheme shown in Fig 1. As in the 2P model in the text (which we call the "original" 2P model), each head of myosin adopts a non-equivalent role. In particular, if one head assumes an actin-dependent role, it may bind to actin and hydrolyze ATP through the actin-dependent pathway at rate k_T. While that head is in the actin-dependent role, its partner head assumes a non-/weak-binding role, where myosin hydrolyzes its ATP only at its basal, actin-independent rate, k_n. The heads switch roles while detached from actin at rate k_s. In the alternative 2P model, unlike the original 2P model, the heads may switch roles while weakly bound to actin at rate k'_s.

Parameter estimates (data from Rovner et al. 2006)

	Original 2P model		Alternative 2P model	
Parameters		Δ_{95}		Δ_{95}
k_s (s^{-1})	$1 \cdot 10^{-4} \pm 0.1$	0-0.22	$4 \cdot 10^{-4} \pm 0.1$	0-0.22
k'_s (s^{-1})	0	–	$8 \cdot 10^{-4} \pm 0.45$	0-0.9
k_T (s^{-1})	4.5 ± 0.4	3.8-5.3	4.5 ± 0.4	3.7-5.5
k_n (s^{-1})	0.11 ± 0.04	0-0.17	0.11 ± 0.04	0-0.17
K_m (μM)	24 ± 4	17-34	23 ± 5	16-36

The alternative 2P model fits the data as well as the original model, where role switching is not allowed while weakly bound (fits not shown). The best fit parameters, and indeed their sensitivity ranges (e.g. the 95% confidence interval Δ_{95}, see Section 3) are nearly identical for the two models (see Table 1). Therefore, the conclusions of the paper (that the two heads have distinct roles and switch these roles slowly, and that smooth muscle may be activated by a phosphorylation dependent equilibrium between active and inactive states) are independent of whether role switching occurs during weak binding or not. For simplicity, we assume that it does not, because we may then neglect the parameter k'_s.

2 Fitting Procedure

In this section, we describe our fitting procedure for each of the various models. As the basic process is the same for each, we first consider a generic kinetic model, and refer to a particular model at the end.

Assuming that myosin can exist in an arbitrary number of states (S), we define the probability of finding a molecule in the i^{th} state at time t as $n_i(t)$. Assuming that all reactions in solution are either first order or

pseudo first order, the rate of change of this state vector is

$$\frac{d\boldsymbol{n}}{dt} = \boldsymbol{A}\boldsymbol{n} \tag{2.1}$$

where $\boldsymbol{A}$ is an $S \times S$ matrix of rate constants that depends on the experimental conditions.

In an open system, where mass leaks out, it can be shown that the matrix $\boldsymbol{A}$ is invertible, and consequently the steady-state solution to Eq. 2.1 is trivial. Alternatively, in a closed system, where mass is conserved, it can be shown that the matrix $\boldsymbol{A}$ is not invertible, and consequently Eq. 2.1 has a non-trivial steady-state solution. If the chemical reaction network is fully connected, meaning that there is a particular set of chemical transformations with non-zero reaction rates that connects any two states in the network, this steady-state is unique (1).

2.1 Single ATP turnover

Single ATP turnover experiments represent open systems, since as fluorescent ATP is hydrolyzed, those myosin heads are no longer detectable and so leave the system. The matrix of rate constants for these experiments, $\boldsymbol{A}_{to}$, is therefore invertible. We may then write the following solution to the differential equation Eq. 2.1:

$$\boldsymbol{n}(t) = \boldsymbol{S}\exp(\boldsymbol{\Lambda}t)\boldsymbol{S}^{-1}\boldsymbol{n}(0) \tag{2.2}$$

where $\boldsymbol{S}$ and $\boldsymbol{\Lambda}$ are the standard eigenvector and eigenvalue matrices of $\boldsymbol{A}_{to}$, respectively.

Eq. 2.2 provides an expression for the probability of finding myosin in any of its S possible states, but the experimentally measured quantity is fluorescence. We therefore define a relative fluorescence vector, $\boldsymbol{f}$, whose i^{th} entry f_i is the relative fluorescence of the i^{th} state (normalized such that the initial fluorescence is 1). Then, the fluorescent signal may be written as

$$F(t) = \boldsymbol{S}\exp(\boldsymbol{\Lambda}t)\boldsymbol{S}^{-1}\boldsymbol{n}(0)\cdot\boldsymbol{f} \tag{2.3}$$

thus, given a matrix of rate constants $\boldsymbol{A}_{to}$, an initial condition vector $\boldsymbol{n}(0)$ and a relative fluorescence vector $\boldsymbol{f}$, we may predict the decay of fluorescence as a function of time, $F(t)$. Note that we may rewrite Eq. 2.3 as the sum of S exponentials

$$F(t) = \sum_{j=1}^{S} A_j e^{-\lambda_j t}$$

where λ_j is the j^{th} eigenvalue, and the sum of all of the A_j's is one. Note that some of the A_j's may be negative or greater than 1. In our simulations, given a set of rate constants, we derived the appropriate matrix of rate constants $\boldsymbol{A}_{to}$ and used Eq. 2.3 to fit the single turnover data of Ellison et al. (2) and Rovner et al. (3). This fitting procedure is described in detail later in this section.

2.2 Steady-state ATPase

Steady-state ATPase experiments represent closed systems, since the concentration of myosin remains constant throughout the experiment. Consequently the matrix of rate constants for these experiments, $\boldsymbol{A}_{ss}$ is not invertible. Thus, for any fully connected reaction network (as all of the models considered here are), we have a unique solution to the steady-state of Eq. 2.1

$$\boldsymbol{A}_{ss}\boldsymbol{n}_{ss} = 0$$

and the solution is

$$\boldsymbol{n}_{ss} = \text{null}(\boldsymbol{A}_{ss})$$

In steady-state ATPase experiments, the rate of ATP turnover is measured indirectly by the concentration of hydrolysis products. We may define a vector, $\boldsymbol{k}$, whose i^{th} entry gives the rate of the particular hydrolysis product formation from state i. Then, the ATPase rate, V_{ATP} is

$$V_{ATP} = \text{null}(\boldsymbol{A}_{ss})\cdot\boldsymbol{k} \tag{2.4}$$

Note that often, for a specific model, simplifications of this equation may be made; however, we used the full Eq. 2.4 for our numerical fits. In our simulations, given a set of rate constants, we derived the appropriate matrix of rate constants $\boldsymbol{A}_{ss}$ and used Eq. 2.4 to fit the steady-state ATPase data of Rovner et al. (3), Ellison et al. (4). We now describe this fitting procedure.

2.3 Numerical optimization of fit

Given a reaction scheme, we may write symbolic expressions for the matrices $\boldsymbol{A}_{to}$ and $\boldsymbol{A}_{ss}$, as well as for the vectors $\boldsymbol{f}$, $\boldsymbol{n}(0)$ and $\boldsymbol{k}$. Then, using Eq. 2.3 and Eq. 2.4, we can solve for the fluorescent decay for the ATP turnover experiments, and the measured steady-state ATPase rate at various actin concentrations. However, the single ATP turnover data are presented as parameters of a double-exponential fit to the fluorescent decay curves, rather than the fluorescent decay curves themselves (2, 3). Thus, in order to fit the data, we must convert the modeled fluorescent decay curve into a double exponential. To perform this conversion, we used a double exponential to fit to the simulated fluorescent decay curve (Eq. 2.3).

We used a Nelder-Mead simplex algorithm (matlab's fminsearch function) to find the double exponential that minimized the least-squared error to the simulated fluorescent decay curve. We used a slightly higher number of points than reported in the data (our simulated data were sampled at ≈ 30 Hz for 30 seconds), in order to ensure that the best-fit exponentials varied as smoothly as possible (an important factor in numerical optimization is that objective functions are smooth). Therefore, given a set of parameters $\boldsymbol{p}$, we can generate a fluorescence decay curve and fit that curve with a double exponential. Comparing the parameters of this best-fit double exponential from the model to those measured in experiment (2, 3), and concurrently fitting the steady-state ATPase curves using Eq. 2.4, we may determine a scalar χ^2 value for the parameter set $\boldsymbol{p}$. Then, we may use an optimization algorithm to find the specific parameter set, $\boldsymbol{p}^*$, that minimizes the χ^2 value.

We used a Nelder-Mead simplex algorithm (Matlab's fminsearch function) to find the optimum parameter set $\boldsymbol{p}^*$. We ensured that the fits converged to the optimum solution by finding each optimum at least twice from initial random seeds. Note that each function evaluation (i.e. each calculation of χ^2 for a given parameter set $\boldsymbol{p}$) requires an optimization since the best double exponential fit must be found, so that these optimizations are rather time-intensive. Thus, we also use simple models that do not require the first optimization to further support our conclusions from the full model (see Section 6).

2.4 Calculating matrices of rate constants

A detailed description of determining rate constant matrices for arbitrary chemical reaction networks is available elsewhere (e.g. 1). Here, we limit ourselves to the specific example of the HMM-2P model (see Fig. 2 of the main text for the model and definitions of the various rate constants) as the basic principles are the same for all models.

To derive an expression for $\boldsymbol{A}_{to}$, the rate constant matrix for the single ATP turnover experiments, we consider a fluorescent ATP molecule bound to one of myosin's two heads. Here, we consider head A (see text Fig. 2). As the labeling of the heads is arbitrary, we need not consider head B separately, and therefore it is sufficient to consider only head A.

We must label the states in which head A may exist while bound to fluorescent ATP. First, it could be in the actin-dependent role while bound to actin. We define the probability that head A is in this state to be n_1. Second, it could be in the actin-dependent role while unbound from actin. This probability is defined as n_2. Third, it could be in the non-/weak-binding role while head B is unbound from actin, with probability n_3. And finally, it could in the non-/weak-binding role while head B is bound to actin, with probability n_4. Note that we have simply numbered the states in text Fig. 2 in a clockwise manner, starting from the lower left.

Looking at, say, state 2, we may write a differential equation relating the rate of change of the probability that a head A is in state 2 to the probability that head A is in that and the other three states:

$$\frac{dn_2}{dt} = k_d n_1 - (k_a[A] + k_n + k_s)n_2 + k_s n_3 \tag{2.5}$$

we may do the same for all other states, and get the following matrix in Eq. 2.1:

$$\boldsymbol{A}_{to} = \begin{bmatrix} -(k_T + k_d) & k_a[A] & 0 & 0 \\ k_d & -(k_n + k_a[A] + k_s) & k_s & 0 \\ 0 & k_s & -(k_s + k_n + k_a[A]) & k_d + k_T \\ 0 & 0 & k_a[A] & -(k_n + k_T + k_d) \end{bmatrix}$$

Note that the detachment rate for state 4 is larger than the detachment rate for state 1, since hydrolysis of head B's ATP results in detachment.

To derive an expression for $\boldsymbol{A}_{ss}$, the rate constant matrix for steady-state ATPase experiments, rather than keeping track of the fluorescent ATP, we keep track of the myosin head (since a head binds multiple ATP molecules). Again, we keep track of head A. We use the same state numbering scheme as for single ATP turnover. Now, however, when we look at state 2, we find

$$\frac{dn_2}{dt} = (k_d + k_T)n_1 - (k_a[A] + k_s)n_2 + k_s n_3 \tag{2.6}$$

Note that, compared to the similar expression for ATP turnover (Eq. 2.5), the detachment rate from state 1 is increased. This difference arises because in single turnover, ATP hydrolysis and subsequent release of hydrolysis products causes the molecule to cease being fluorescent, while the molecule is always detectable in steady-state ATPase. Similarly, when the molecule in state 2 hydrolyzes ATP, it leaves the system in the turnover experiments, but not the steady-state ATPase experiments. Thus, we derive the following matrix for steady-state ATPase experiments

$$\boldsymbol{A}_{ss} = \begin{bmatrix} -(k_T + k_d) & k_a[A] & 0 & 0 \\ k_d + k_T & -(k_a[A] + k_s) & k_s & 0 \\ 0 & k_s & -(k_s + k_a[A]) & k_d + k_T \\ 0 & 0 & k_a[A] & -(k_T + k_d) \end{bmatrix}$$

Note that all of the rows sum to the zero vector, indicating that $\boldsymbol{A}_{ss}$ is not invertible, as expected.

We also need expressions for $\boldsymbol{f}$, $\boldsymbol{n}(0)$ and $\boldsymbol{k}$ in order to fit the 2P model to a data set. We assume that, since mant d-ATP (or fluorescent ATP) or hydrolysis products are in the binding pocket for all states in the single ATP turnover model, $\boldsymbol{f}$ is simply a vector of ones, as all states are equally fluorescent. We assume that at the beginning of the single ATP turnover experiment all myosin is unbound from actin, and half of the molecules have head A in the actin-dependent role. Finally, the rate of ATP hydrolysis vector, $\boldsymbol{k}$, for the turnover model can be determined directly from Fig. 2 in the manuscript. Thus we have

$$\boldsymbol{f} = \begin{bmatrix} 1 \\ 1 \\ 1 \\ 1 \end{bmatrix} \quad \boldsymbol{n}(0) = \begin{bmatrix} 0 \\ \frac{1}{2} \\ \frac{1}{2} \\ 0 \end{bmatrix} \quad \boldsymbol{k} = \begin{bmatrix} k_T + k_n \\ 2k_n \\ 2k_n \\ k_T + k_n \end{bmatrix}$$

3 Sensitivity analysis

In order to estimate parameters from a numerically optimized fit to data, one must have some idea of the error associated with each parameter given by the optimization. There are a variety of different ways to estimate this error. Perhaps the most accurate estimate is achieved by performing a series of optimizations keeping one parameter fixed and using the optimization algorithm to determine the values of the remaining variables that minimize the chi squared error between model and data. As the fixed parameter is varied over some range, a curve of minimum chi square value as a function of that parameter value is generated, with a minimum at the optimum value (the result of the global optimization, See Figs. 2 and 3). One may then estimate standard deviation (σ), 95% (Δ_{95}) and 99% (Δ_{99}) confidence intervals. Note that, while we make every effort to ensure the optimization converges at each point, this convergence is not guaranteed. Therefore, in section 6, we introduce simplified models that support the conclusions of the full numerical optimization.

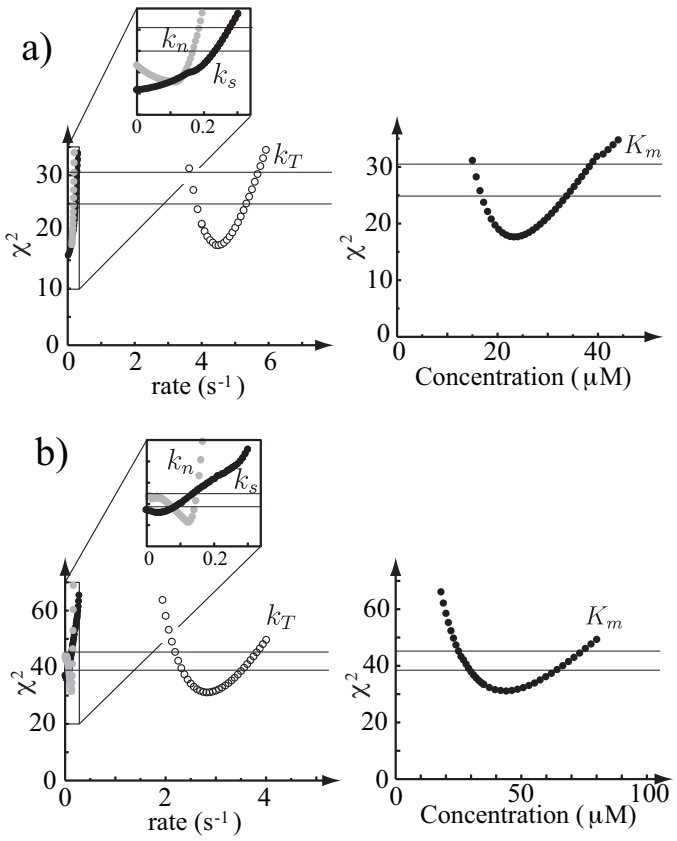

Figure 2: Sensitivity analysis for 2P myosin. Plots of goodness-of-fit (χ^2) as a function of the reduced parameters (k_s, k_n, k_T and K_m). Each point in these plots represents an optimization with a single reduced parameter (say, k_s) fixed at the given value, while the remaining parameters (k_n, k_T and K_m) are varied to optimally fit single turnover and steady-state ATPase data. These plots allow us to determine a 95% confidence interval (by finding the intersections with the bottom horizontal line) and a 99% confidence interval (by finding the intersections with the top line). a) The data of Rovner et al. (3) were fit with the 2P model. b) The data of Ellison et al. (4) and Ellison et al. (2) were fit.

3.1 Sensitivity of reduced parameters in the 2P model

We performed a sensitivity analysis on the parameters of the 2P model. We found, however, that the parameters k_a and k_d could vary over many orders of magnitude. Indeed, values of $k_d = O(10^{-3})$ and $k_d = O(10^8)$ both can fit the data ($p > 0.05$, chi square test). However, the model is sensitive to the combination of parameters $K_m = (k_T + k_d)/k_a$. Thus, we report this value, and the error associated with it. The reason for this parameter insensitivity is discussed in Section 6.

In Table 1, we estimate standard deviation (σ), a 95% confidence interval (Δ_{95}) and a 99% confidence interval (Δ_{99}). We estimate the standard deviation as one quarter of the size of the 95% confidence interval. This estimate assumes that the distribution is Gaussian, which is approximately correct over small intervals, but questionable over larger ones (see Fig. 2).

2P Model Confidence Intervals

	Rovner et al. 2006			Ellison et al. 2000, 2003		
Parameters	σ	Δ_{95}	Δ_{99}	σ	Δ_{95}	Δ_{99}
k_s (s^{-1})	0.11	0-0.22	0-0.26	0.02	0-0.09	0-0.15
k_T (s^{-1})	0.4	3.8-5.3	3.7-5.7	0.4	2.3-3.5	2.2-3.8
k_n (s^{-1})	0.04	0-0.17	0-0.19	0.02	0.08-0.14	0-0.15
K_m (μM)	4	17-34	15-38	8	$30-64$	25-74

3.2 Sensitivity of reduced parameters in the 1P and 2P models

We performed a sensitivity analysis on the parameters of the 1P and 2P models simultaneously (see Fig. 3). Like in the 2P model, we found that some parameters (k_a, k_d, k_a^*, k_d^*, k_2, k_3, k_2' and k_3') could vary over many orders of magnitude. Again, we found that the model is sensitive to combinations of parameters (see Section 6). In particular, the parameters $a_1 = 1/(1 + k_2/k_3)$, $a_2 = 1/(1 + k_2'/k_3')$, $K_m = (k_T + k_d)/k_a$ and $K_m^{1P} = (a_2 k_T + k_d^{eff})/k_a^{eff}$. Where the effective attachment rate (k_a^{eff}) is defined as $k_a^{eff} = a_1 k_a + (1-a_1)k_a^*$ and the effective detachment rate (k_d^{eff}) is defined as $k_d^{eff} = a_2 k_d + (1-a_2)k_d^*$. Thus, we report these value, and the error associated with them.

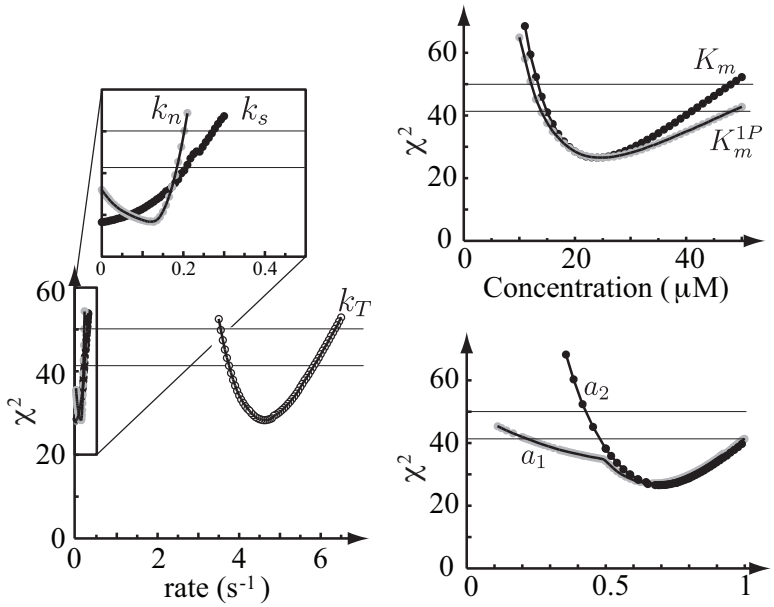

Figure 3: Sensitivity analysis of the reduced parameters of the 1P and 2P models. Plots of goodness-of-fit (χ^2) as a function of the reduced parameters (k_s, k_n, k_T, a_1, a_2, K_m and K_m^{1P}). Each point in these plots represents an optimization with a single reduced parameter (say, k_s) fixed at the given value, while the remaining parameters (k_n, k_T, a_1, a_2, K_m and K_m^{1P}) are varied to optimally fit single turnover and steady-state ATPase data for both 1P and 2P myosin. These plots allow us to determine a 95% confidence interval (by finding the intersections with the bottom horizontal line) and a 99% confidence interval (by finding the intersections with the top line). The data of Rovner et al. (3) were fit with the 2P and 1P models.

Note that in these fits, we may define a 68% confidence interval, which defines an equivalent standard deviation. When the curves are clearly non-Gaussian (e.g. a_1, see Fig. 3), this method provides a more accurate estimate of standard deviation than estimates based on one quarter of the size of the 95% confidence interval. In all other cases, however, both estimation techniques agreed.

1P Model Confidence Intervals

Parameters	σ	Δ_{95}	Δ_{99}
k_s (s^{-1})	0.1	0-0.2	0-0.26
k_T (s^{-1})	0.5	3.8-5.8	3.5-6.4
k_n (s^{-1})	0.05	0-0.19	0-0.2
K_m (μM)	7	15-41	14-48
a_1	0.14	0.22-1	0-1
a_2	0.14	0.15-1	0.42-1
K_m^{1P} (μM)	9	14-48	12-60

4 Actin-dependent 2P models

Numerical optimization of our kinetic model for doubly-phosphorylated (2P) myosin shows that the two heads have distinct roles (actin-dependent and non-binding) and they switch these roles slowly. This conclusion is largely based on the observation that single ATP turnover data is well-fit by double exponentials of approximately equal magnitude. Our model assumes that these two roles exist whether or not actin is associated with myosin. Here, we consider two alternate models where actin is required to determine the roles. We will show that these models are inconsistent with steady-state ATPase and single ATP turnover data (2–4).

4.1 The actin-associated model

In the first alternate model, which we call the actin-associated model, the two heads while detached are indistinguishable and equally likely to attach to actin. It is only upon attachment to actin that the roles of the two heads are determined. In particular, the first head to bind assumes the actin-associated role, while the other head assumes the weak/non-binding role. Upon release of hydrolysis products and subsequent rebinding of ATP, the myosin molecule must not completely detach from actin or else the model becomes the model presented in the main text, with $k_s \to \infty$ (see Fig. 2 of main text). Therefore, upon release of hydrolysis products and binding of a fresh ATP molecule, myosin does not fully detach, and the actin-associated head may perform additional productive ATP hydrolysis cycles. Consequently, the non-/weak-binding head remains sterically inhibited from undergoing a productive cycle. This model is sketched in Fig. 4b.

Numerical optimization of the fit of this model to the single ATP turnover and steady-state ATPase data of Rovner et al. (3), generates best fits that are significantly different from the data ($p < 0.001$). The model also differs significantly from the data of Ellison et al. (4) and Ellison et al. (2) ($p < 0.001$). The major difference between the model and the data is that the model predicted a K_m about an order of magnitude too small (see Fig. 5). For this model, we can derive a simplified model that explains why the K_m is too small, and why this model cannot fit the data (see Section 4.3). We therefore reject this model.

4.2 The double head binding model

In the second model, which we call the double head binding model, the two heads while detached are indistinguishable and equally likely to attach to actin. Like the actin-associated model, the first head to bind assumes the actin-associated role, while the other head assumes the weak/non-binding role. However, in this model, the second head may then assume an actin-associated role. Intermolecular strain may affect the rates of the heads differentially, depending on their relative position (5, 6). Thus, the lead head might hydrolyze ATP slowly, while the rear head hydrolyzes ATP quickly in an actin-independent manner. This model is sketched in Fig. 4a.

Using numerical optimization to fit this model to the single ATP turnover and steady-state ATPase data of Rovner et al. (3), generated best fits that were significantly different from the data ($p < 0.01$). In particular, although the model could fit the steady-state ATPase data, and the rates of the single turnover data, it was unable to fit both simultaneously (see Fig. 5). The model also differed significantly from the data of Ellison et al. (4) and Ellison et al. (2) ($p < 0.001$), especially the steady-state ATPase (see Fig. 5). Furthermore, we expect that the binding of the second head should accelerate the ATP hydrolysis rate of

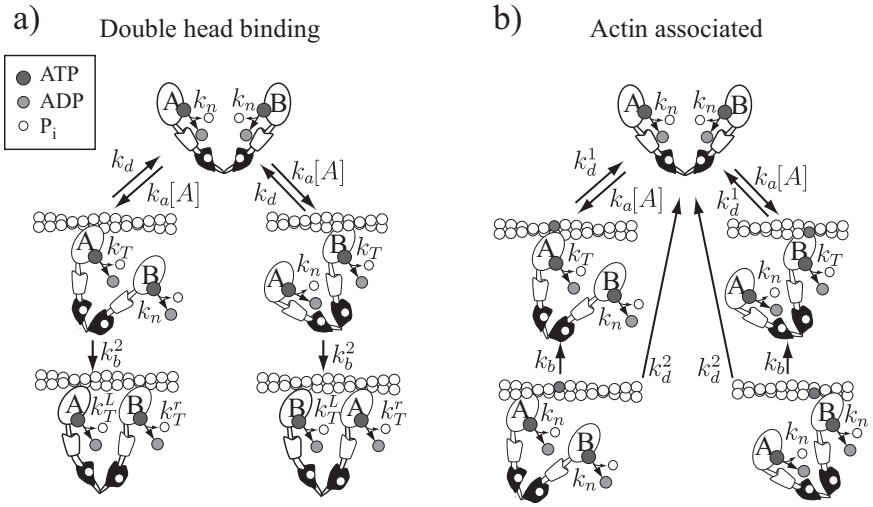

Figure 4: Sketches of the two actin-dependent 2P models. In each model, while detached from actin, the two heads are indistinguishable, and may assume an actin-dependent role, where ATP may be hydrolyzed through the actin-dependent pathway with rate constant k_T, with equal likelihood. a) In the double head binding model, after the first head assumes an actin-dependent role, the second head may also assume an actin-dependent role. The presence of intermolecular strain changes the actin-activated ATPase rate from k_T to k_T^L for the lead head and k_T^r for the rear head. b) In the actin-associated model, after ATP hydrolysis, myosin does not fully detach from actin. Thus, once a particular head strongly binds, it is more likely than its partner head to assume the actin-dependent role in a subsequent interaction. Neither the double head binding nor the actin associated model can fit the single ATP turnover and steady-state ATPase data of Rovner et al. (3) or the single ATP turnover and steady-state ATPase data of Ellison et al. (4) and Ellison et al. (2).

the rear head (k_T^r) and slow the ATP hydrolysis rate of the lead head (k_T^L). Thus, if this model were correct, we would expect the singly bound ATPase rate (k_T) to be intermediate between those values (k_T^L and k_T^r). The optimum values do not support this conclusion. Therefore, we reject this model.

4.3 Simplifications of the actin-associated model

While numerical optimizations are a useful way of testing complex models, it is very hard to guarantee that the optimum fit is found. Thus, if a given model does not fit the data, we must face the criticism that the optimum fit was simply not found by the optimization. While we may minimize the probability that unfound optima exist by running numerous optimizations from random seeds and ensuring that each optimum is found many times, we may not entirely eliminate this alternative unless we can show that the model is incapable of fitting the data. Here, based on some plausible arguments, we present a simplified model for the actin-associated model to show why it cannot fit the data, supporting the result from numerical optimization. Based on this result, we may confidently reject the actin-associated model.

We make two assumptions that simplify the model considerably. First, we note that if the rate of actin dissociation from the first bound state, k_d^1, is large compared to the actin-activated ATP turnover rate k_T, then the two heads will switch roles quickly (see Fig. 4b). Since the single turnover data implies that the heads switch roles slowly, we assume that k_d^1 is small compared to k_T. Second, if this model is to explain the single ATP turnover data, then a single head must go through numerous ATP hydrolysis cycles per binding event. Therefore, we assume that the rate of unbinding from the second bound state, k_d^2, must be less than the transition rate to the first bound state k_b (see Fig. 4b). Therefore, we expect that both k_d^1 and k_d^2 are small when compared to the sum $k_b + k_T$.

In addition to the assumption that the dissociation rates are small, we assume that the ATP hydrolysis rate of the bound head is so much greater than that of the unbound head (k_n) that k_n can be neglected.

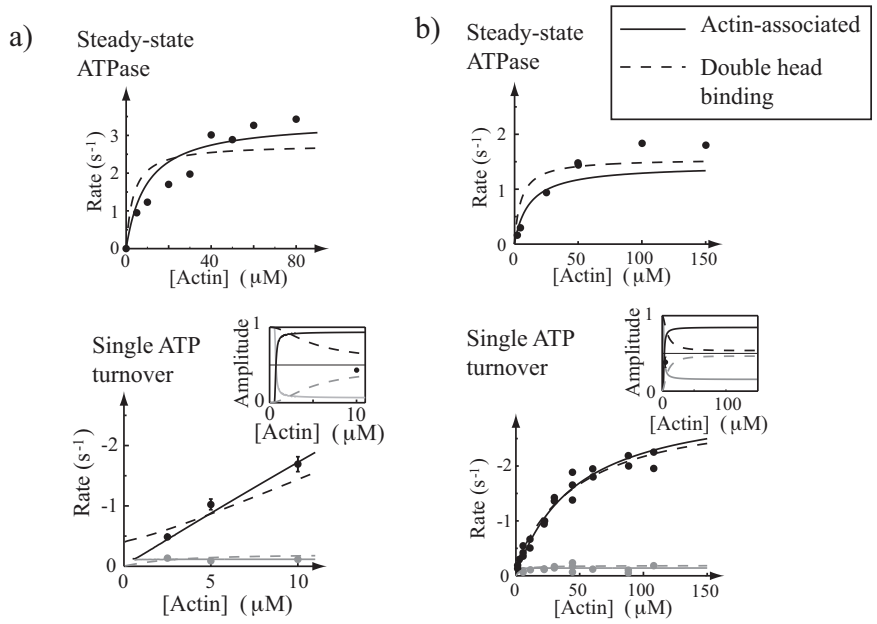

Figure 5: The actin-dependent models do not fit steady-state and single turnover ATPase experiments. Solid lines are the best-fits from the actin-associated model; dashed lines are the best-fits from the double head binding model. a) The data of Rovner et al. (3) b) The data of Ellison et al. (4) and Ellison et al. (2)

Given these assumptions and using the techniques outlined in the Section 2, Fitting Procedure, we may write a few important analytic expressions.

First, we must find an expression for the rate that the heads switch roles (k_{switch} in our simplified model of head-head interactions in Section 5). In the actin-associated model, k_{switch} is half the rate at which a bound head unbinds, since half the time that same head will subsequently rebind, and therefore not switch its role. In general, however, a bound head unbinds at two rates (i.e. the unbinding rate is the sum of two exponentials), which we call r_1 and r_2, that may be written

$$r_{1,2} = \frac{k_b + k_T + k_d^1 + k_d^2}{2} \mp \sqrt{\frac{(k_b + k_T + k_d^1 + k_d^2)^2}{4} - (k_T + k_d^1)(k_b + k_d^2) + k_b k_T}$$

If we take the limit of small k_d^2, k_d^2, we find that $r_1 \to 0$ and $r_2 \to k_b + k_T$. Since, at small k_d^1 and k_d^2, we expect the switching rate to approach zero (i.e. be much smaller than $k_b + k_T$), the amplitude of the exponential with rate r_1 must be dominant at small k_d^2, k_d^2. Thus, expanding the expression for r_1 in a Taylor series, we find

$$2k_{switch} = r_1 = \left(\frac{k_b}{k_b + k_T}\right) k_d^1 + \left(\frac{k_T}{k_b + k_T}\right) k_d^2 + O\left(\frac{k_d^{1,2}}{(k_b + k_T)}\right)$$

With our assumption that $k_d^1, k_d^2 \ll k_b + k_T$, we may neglect the higher order terms. Since this switching rate must be slow (the 95% confidence interval $\Delta_{95} = 0.06\text{-}0.3\text{s}^{-1}$, see Section 5), we assume that it is less than 0.3s^{-1}.

$$k_{switch} \approx \left(\frac{k_b}{k_b + k_T}\right) \frac{k_d^1}{2} + \left(\frac{k_T}{k_b + k_T}\right) \frac{k_d^2}{2} < 0.3\text{s}^{-1} \tag{4.1}$$

Then, using an eigenvalue calculation to find the rates, and then performing a Taylor expansion in actin concentration keeping only the linear terms (see the reduced model in Section 6), we can find a relation for the slope of the faster actin-dependent rate (ℓ_1) in the double-exponential fit:

$$-\frac{d\ell_1}{d[A]} = \frac{k_T k_a}{k_d^1 + k_T} \approx 0.15 \pm 0.05\text{s}^{-1}\mu\text{M}^{-1} \tag{4.2}$$

where the numeric value comes from a best-fit to the turnover data of Rovner et al. (3) (points read off a digital PDF of their Fig. 5a).

Finally, we may fit the steady-state turnover data to an equivalent Michaelis-Menten curve. We start by using the general equation of Section 2 (Eq. 2.4). Then, defining V_{max} as the limit of this equation as $[A] \to \infty$, we find

$$V_{max} = \frac{k_T(k_b + k_d^2)}{k_b + k_d^2 + k_T} = 4.8 \pm 0.6\text{s}^{-1} \tag{4.3}$$

where the numeric value comes from the measurements of Rovner et al. (3). We note that, in a Michaelis-Menten curve, the initial slope is $dV_{ATP}/d[A] = V_{max}/K_M$. Thus, we may determine K_M from this initial slope and V_{max}, which gives the following expression:

$$K_M = \frac{k_d^1 k_d^2 + k_T k_d^2 + k_b k_d^1}{k_a(k_b + k_d^2 + k_T)} = \frac{V_{max}}{k_a}\left(\frac{k_d^2}{k_b + k_d^2} + \frac{k_d^1}{k_T}\right) = 32 \pm 10\mu\text{M} \tag{4.4}$$

where, again, the numerical values come from a Michaelis-Menten fit to steady-state ATPase data (3).

Therefore, if the data are to be explained with the actin-dependent complex model, then we must pick rate constants such that the four constraints, Eq's 4.1 – 4.4 are satisfied.

However, any choice of parameters that satisfies Eq's 4.1 – 4.3 and our assumptions deriving them, is inconsistent with Eq 4.4. In particular, assuming that $k_d^1, k_d^2 \ll k_T + k_b$, we may rearrange Eq. 4.3 to be

$$\frac{V_{max}}{k_b + k_d^2} \approx \frac{k_T}{k_b + k_T}$$

and, plugging this expression into Eq. 4.1, we have

$$\frac{1}{2}\left[k_d^1\left(\frac{V_{max}}{k_T} - \frac{k_d^2}{k_b + k_T}\right) + k_d^2\frac{V_{max}}{k_b + k_d^2}\right] \approx \frac{V_{max}}{2}\left(\frac{k_d^1}{k_T} + \frac{k_d^2}{k_b + k_d^2}\right) < 0.3\text{s}^{-1}$$

from Eq. 4.2, we may write

$$k_a \geq 0.15 \pm 0.05\text{s}^{-1}\mu\text{M}^{-1}$$

so that, combining the previous two expressions, we may write

$$\frac{V_{max}}{k_a}\left(\frac{k_d^1}{k_T} + \frac{k_d^2}{k_b + k_d^2}\right) < \frac{0.6}{0.15 \pm 0.05}\mu\text{M}$$

which is the expression for K_M in Eq. 4.4

$$K_M < 4 \pm 1.5\mu\text{M}$$

which, even assuming the maximum value, is significantly different from the measured value, $K_M = 32 \pm 10\mu$M (Student's t-test, $p < 0.001$).

Thus, we see that if the model fits the single ATP turnover data of Rovner et al. (3), the model becomes unable to fit the steady-state ATPase data. In particular, it binds too strongly to actin, leading to an overly low K_M. These predictions are consistent with the numerical fits.

5 Slow switching rate arguments

In the main text, and in Section 3, we use numerical optimizations to argue that the rate of role switching k_s must be slow in both the 2P and 1P models. One problem with numerical optimization is that it is unclear what aspects of the data determine parameter values. Thus, in some cases, small systematic errors can lead to wildly incorrect parameter estimates. In this section, we use various simplifications to identify the aspects of the single ATP turnover data that determine the switching rate. We show that several independent aspects of the data (e.g. signal amplitude and signal rates) all point to slow switching. Thus, we conclude that in order to explain single ATP turnover measurements of Rovner et al. (3) and Ellison et al. (2) the slow switching is unavoidable.

5.1 Small actin approximations

Here, we show that the behavior of the kinetic models at small actin concentrations implies slow switching. In particular we use the methods described in Section 2 to show that the fluorescence in the 2P model decays according to the equation

$$F(t) = A_1 e^{\lambda_1 t} + A_2 e^{\lambda_2 t} + A_3 e^{\lambda_3 t} + A_4 e^{\lambda_4 t} \tag{5.1}$$

where λ_i is the i^{th} eigenvalue of the matrix $\boldsymbol{A}_{to}$ defined in that section. The four eigenvalues satisfy the following relation (e.g. that $\det(\boldsymbol{A}_{to} - \lambda_i \boldsymbol{I}) = 0$):

$$\begin{aligned}[-(k_n + k_a[A] + k_s + \lambda_i)\left((k_s + k_n + k_a[A] + \lambda_i)(k_n + k_T + k_d + \lambda_i) - k_a[A](k_d + k_T)\right) + \cdots \\ k_s^2(k_n + k_T + k_d + \lambda_i)\big]\,(k_T + k_d + \lambda_i) + \cdots \\ -k_a[A]\left[k_d\left((k_s + k_n + k_a[A] + \lambda_i)(k_n + k_T + k_d + \lambda_i) - k_a[A](k_d + k_T)\right)\right] = 0\end{aligned}$$

which is quartic in λ_i, and so in general has no analytic solution. However, when the concentration of actin approaches zero, we may solve explicitly for the exponential rates λ_i:

$$\begin{aligned}\lim_{[A]\to 0} \lambda_1 &= -k_n \\ \lim_{[A]\to 0} \lambda_2 &= -k_n - 2k_s \\ \lim_{[A]\to 0} \lambda_3 &= -k_d - k_T \\ \lim_{[A]\to 0} \lambda_4 &= -k_d - k_T\end{aligned}$$

Additionally, at the other extreme, as $[A]$ becomes large we find $\lim_{[A]\to\infty} \lambda_1 = -k_T$ and $\lim_{[A]\to\infty} \lambda_2 = -k_n$.

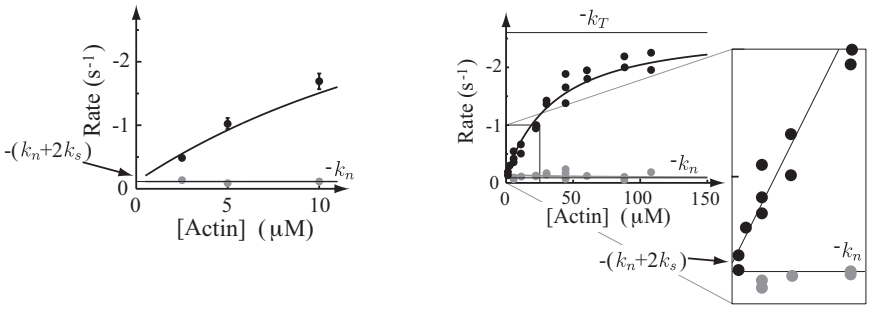

Figure 6: One demonstration of why the 2P model requires slow role switching. At low actin concentrations, we predict that the faster, actin-dependent rate approaches $-(k_n + 2k_s)$, while the slower, actin-independent rate approaches $-k_n$ (see text for derivation). We may then estimate the switching rate, k_s, as half the extrapolated difference between the two curves at $[A] = 0$. From the experimental curves (Rovner et al. (3), left and Ellison et al. (4), right)) it is clear that k_s is small.

The steady-state ATPase measurements allow us to estimate $k_T \approx 4.5 s^{-1}$ for measurements from the Trybus lab (3) and $k_T \approx 2.6 s^{-1}$ for measurements from the Cremo lab (2, 4). We also expect that $k_n \approx 0.1 s^{-1}$ (3), an order of magnitude smaller than k_T. We note that ℓ_1, the measured actin-dependent rate, starts from a small value and approaches $-k_T$. We further note that ℓ_2, the measured actin-independent rate, remains small at all actin concentrations. Thus, assuming that the parameters of the double exponential fits (e.g. the rates ℓ_1, ℓ_2 and amplitudes $\mathcal{A}_1$, $\mathcal{A}_2$) relate simply to the parameters of the full model (Eq. 5.1), we may identify the two rates $\ell_1 = \lambda_1$ and $\ell_2 = \lambda_2$. Thus, if we extrapolate back to $[A] = 0$, we may estimate $k_s = (\ell_1 - \ell_2)/2$. This procedure provides an estimate of $\Delta_{95} = 0\text{-}0.2 s^{-1}$ for both preparations of HMM-2P, in reasonable agreement with the full numerical fit. As ℓ_1 and ℓ_2 clearly approach each other closely at small actin concentrations (see Fig. 6), k_s must be small, supporting the conclusion of the numerical optimization.

5.2 Signal amplitudes

Here, we show that having roughly equal signal amplitudes for the two non-equal rates of ATP turnover implies slow role switching. We also provide an explanation for why the data of Ellison et al. (2) imply a small but non-zero rate, while that of Rovner et al. (3) can be explained with zero switching rate.

Here, we take a more simplistic view of single ATP turnover than previously. In this simple model, we may exactly determine how switching rate affects signal amplitude. We then argue that, since the more complex model shares many of the features of the simple model, the results of the simple model hold for the more complex one.

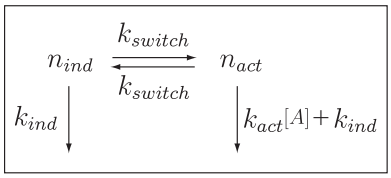

Figure 7: A simple model that demonstrates how roughly equal amplitudes in the double-exponential fit to fluorescence decay implies slow role switching. We assume two populations of heads. One (n_{ind}) hydrolyzes ATP through the actin-independent pathway at rate k_{ind}. The other (n_{act}) hydrolyzes ATP through the actin-dependent pathway at rate $k_{ind}+k_{act}[A]$. The heads switch roles at rate k_{switch}. We show that, in this model, single ATP turnover fluorescence is the sum of two exponentials, and that the amplitudes of these exponentials are equal only if k_{switch} is small.

We assume that two populations of heads exist. One population hydrolyzes ATP in an actin-independent fashion, at rate k_{ind} (presumably, this rate is similar to k_n). There are $N_h n_{ind}$ heads in this population, where N_h is the total number of heads in the population. The other population hydrolyzes ATP at an actin-dependent fashion, that may be written as $k_{act}[A] + k_{ind}$, at low actin concentrations. There are $N_h n_{act}$ heads in this population. Heads move from one population to the other at a rate k_{switch} (presumably, this rate is similar to k_s). The kinetic scheme is sketched in Fig. 7. We now show that this model predicts a fluorescence decay curve that is the sum of two exponentials and that the amplitudes of these exponentials are strongly dependent on switching rate. Finally, we show that given the measured amplitudes, this model predicts a switching rate k_{switch} that is in good agreement with the switching rate of the full model k_s. Thus, we argue that the equality of the signal amplitudes implies slow switching.

In general, this simple kinetic scheme results in the following system of differential equations (see Eq. 2.1):

$$\frac{d}{dt}\begin{bmatrix} n_{ind} \\ n_{act} \end{bmatrix} = \begin{bmatrix} -(k_{ind}+k_{switch}) & k_{switch} \\ k_{switch} & -(k_{act}[A]+k_{ind}+k_{switch}) \end{bmatrix}\begin{bmatrix} n_{ind} \\ n_{act} \end{bmatrix}$$

provided that $k_{act}[A] \neq 0$, this equation is readily solved (see Eq. 2.2):

$$\begin{bmatrix} n_{ind} \\ n_{act} \end{bmatrix} = \boldsymbol{S}\begin{bmatrix} e^{\lambda_1 t} & 0 \\ 0 & e^{\lambda_2 t} \end{bmatrix}\boldsymbol{S}^{-1}\begin{bmatrix} n_{ind}(0) \\ n_{act}(0) \end{bmatrix}$$

where λ_1 and λ_2 are the eigenvalues of the matrix of rate constants and $\boldsymbol{S}$ is the matrix of eigenvectors.

Since the proportion of myosin with fluorescence bound, n_{tot}, is equal to the relative fluorescence $F(t)$, we wish to find a scalar expression for $n_{tot} = n_{act}+n_{ind}$, given that $n_{ind}(0) = n_{act}(0) = 0.5$. It is straightforward to see that the required expression is:

$$F = \boldsymbol{S}\begin{bmatrix} 1 & 0 \\ 0 & 0 \end{bmatrix}\boldsymbol{S}^{-1}\begin{bmatrix} 0.5 \\ 0.5 \end{bmatrix}\cdot\begin{bmatrix} 1 \\ 1 \end{bmatrix}e^{\lambda_1 t} + \boldsymbol{S}\begin{bmatrix} 0 & 0 \\ 0 & 1 \end{bmatrix}\boldsymbol{S}^{-1}\begin{bmatrix} 0.5 \\ 0.5 \end{bmatrix}\cdot\begin{bmatrix} 1 \\ 1 \end{bmatrix}e^{\lambda_2 t}$$

and so the general form of the solution is

$$F = A_1 e^{\lambda_1 t} + A_2 e^{\lambda_2 t} = \mathcal{A}_1 e^{\ell_1 t} + \mathcal{A}_2 e^{\ell_2 t}$$

a double exponential. Where we use the notation used in the main text, where the first equation (with λ_i and A_i) relates to the eigenvalue calculation above; while the second equation (with ℓ_i and $\mathcal{A}_i$) relates to the

double exponential fit to fluorescence. We may then calculate these amplitudes ($\mathcal{A}_1$ and $\mathcal{A}_2$) and exponents (ℓ_1 and ℓ_2) for arbitrary k_{ind}, $k_{act}[A]$ and k_{switch}.

The eigenvalues are:

$$\ell_1 = k_{switch}\left[-\left(1+\frac{k_{ind}}{k_{switch}}+x\right)+\sqrt{1+x^2}\right]$$
$$\ell_2 = k_{switch}\left[-\left(1+\frac{k_{ind}}{k_{switch}}+x\right)-\sqrt{1+x^2}\right]$$

where $x = k_{act}[A]/2k_{switch}$.

The matrix $\boldsymbol{S}$ is

$$\boldsymbol{S} = \begin{bmatrix} -\frac{1}{\sqrt{1+a_1^2}} & -\frac{1}{\sqrt{1+a_2^2}} \\ \frac{a_1}{\sqrt{1+a_1^2}} & \frac{a_2}{\sqrt{1+a_2^2}} \end{bmatrix}$$

where $a_1 = x - \sqrt{1+x^2}$, $a_2 = x + \sqrt{1+x^2}$. The matrix $\boldsymbol{S}^{-1}$ is

$$\boldsymbol{S}^{-1} = \begin{bmatrix} \frac{a_2\sqrt{1+a_1^2}}{a_1-a_2} & \frac{\sqrt{1+a_1^2}}{a_1-a_2} \\ -\frac{a_1\sqrt{1+a_2^2}}{a_1-a_2} & -\frac{\sqrt{1+a_2^2}}{a_1-a_2} \end{bmatrix}$$

The amplitude $\mathcal{A}_1$ is then

$$\mathcal{A}_1 = \frac{1}{2} - \frac{1}{a_1-a_2} = \frac{1}{2} + \frac{1}{2\sqrt{1+x^2}}$$

and the amplitude $\mathcal{A}_2$ is

$$\mathcal{A}_2 = \frac{1}{2} + \frac{1}{a_1-a_2} = \frac{1}{2} - \frac{1}{2\sqrt{1+x^2}}$$

5.2.1 Data comparisons

Ellison et al. (4) report amplitudes of $\mathcal{A}_1 = 0.618 \pm 0.068$ and $\mathcal{A}_2 = 0.382 \pm 0.068$ at 5μM actin. We may use these measurements to estimate x:

$$x = \frac{k_{act}[A]}{2k_{switch}} = 4.24 \pm 1.73$$

Ellison et al. (2) measured $-\ell_2$, the faster, smaller amplitude rate, as a function of actin concentration. At small $[A]$, this rate is linear in $[A]$. We measured the slope of this line from a PDF of their Fig. 6, and found:

$$-\frac{d\ell_2}{d[A]} = k_{act} = 0.042 \pm 0.01 \mu\mathrm{M}^{-1}\mathrm{s}^{-1}$$

The actin concentration on which our estimate of x is based is 5μM. Thus, we estimate k_{switch} to be

$$k_{switch} = \frac{0.042 \pm 0.01 \cdot 5}{2 \cdot 4.24 \pm 1.73}\mathrm{s}^{-1} = 0.025 \pm 0.013\mathrm{s}^{-1}$$

and thus a 95% confidence interval is Δ_{95} = 0-0.051s^{-1}. From the full model fits to the data, we found a best-fit value of $k_s = 0.063\mathrm{s}^{-1}$ and a 95% confidence interval of Δ_{95} = 0-0.09s^{-1}. These values are in reasonable agreement.

Rovner et al. (3) only report a single amplitude for 2P myosin, but they report a larger amplitude for the faster rate (0.57) than for the slow rate (0.43). The simple model here predicts that the amplitude of the faster rate should never be greater than that of the slower rate. In Section 6, we introduce a simplified model that explains how this situation can occur. Regardless, in order to get a non-zero rate of switching, we need an estimate of signal amplitudes where the amplitude associated with the slower rate is larger. We therefore assume that the amplitude measurements of Ellison et al. (4) apply also to these data.

Rovner et al. (3) measured $-\lambda_2$ and found the rate to be linear in $[A]$ at small $[A]$. We measured the slope of this line from a PDF of their Fig.5a, and found:

$$-\frac{d\ell_2}{d[A]} = k_{ind} = 0.15 \pm 0.05 \mu\mathrm{M}^{-1}\mathrm{s}^{-1}$$

Since we use the amplitude measurements of Ellison et al. (4), we use our previous estimate of x but now note that $[A] = 10\mu$M. Thus, we estimate k_{switch} to be

$$k_{switch} = \frac{0.15 \pm 0.05 \cdot 10}{2 \cdot 4.24 \pm 1.73}\mathrm{s}^{-1} = 0.18 \pm 0.06\mathrm{s}^{-1}$$

and thus a 95% confidence interval is $\Delta_{95} = 0.06\text{-}0.3\mathrm{s}^{-1}$. From the full model fits to the data, we found a best-fit value of $k_s = 1 \cdot 10^{-4}\mathrm{s}^{-1}$ and a 95% confidence interval of $\Delta_{95} = 0\text{-}0.22\mathrm{s}^{-1}$. These values are in reasonable agreement. This good agreement seen for both data sets suggests that the simplified model provides a reasonable approximation of the more complex model.

In the simplified model, the amplitudes of the two exponential rates in the fit to fluorescence provide an estimate for switching rate. The closer the faster amplitude is to 50%, the slower the switching rate. Alternatively, as this amplitude becomes smaller than 50%, the faster the switching rate must be. As Ellison et al. (4) report a faster amplitude smaller than 50%, we expect a non-zero switching rate; since Rovner et al. (3) report a faster amplitude greater than 50%, we cannot rule out a zero switching rate. Thus, we expect the switching rate to be slower for the data of Rovner et al. (3), another prediction that is supported by the data.

Here, we have shown two aspects of the double-exponential fits to the single ATP turnover fluorescence decay curves that necessitate a slow switching rate. First, the close approach of the two rates at low actin concentrations implies that switching must be slow. Second, the rough equality of the signal amplitudes implies that role-switching must be slow. Thus, we may understand and have confidence in the results of the numerical optimization.

6 Simplified models

In the text, we introduce relatively complex models for doubly (2P) and singly (1P) phosphorylated HMM. In particular, for the single ATP turnover experiments, comparison of the model with the data requires two optimizations: first, the predicted fluorescent-time curve is fit with a double exponential, and second, experimental data are fit with the parameters of this exponential fit. Besides making each optimization computationally intensive, these nested optimizations lead to slow convergence.

Here, we introduce simplified models for both 2P and 1P HMM that do not require a double exponential fit. The first, which we call the "analytical fit" model, requires minimal assumptions, fits the data and predicts parameter values as well as the full model, but is still quite complex. The second, which we call the "reduced" model, requires two extra assumptions in addition to those of the analytical fit model, doesn't fit the data or predict parameter values quite as well as the full or analytical fit model, but is very simple. Taken together, these simple models confirm the conclusions of the full model and allow us to understand the results of the full model. In particular, the reduced model provides an intuition for parameter values and explains parameter sensitivity in the full model.

6.1 The analytical fit model for 2P myosin

In the numerical optimization of the full model for 2P myosin (Fig. 2a), we found that the rate at which myosin's two heads switch their roles, k_s, had to be small in order to explain the data. Here, we assume that this rate is precisely zero. While this assumption may not be correct, it allows us to write (relatively) simple expressions for the single ATP turnover experiments.

6.1.1 The fluorescence decay curve in single ATP turnover

Given that $k_s = 0$, we may consider the heads in an actin-dependent role separately from heads in the non-binding role. So, for example, a head in the actin-dependent role turns over ATP at a rate k_n while

unbound, and at a rate k_T while bound. It binds to actin with rate $k_a[A]$ and unbinds from actin at a rate k_d. Using the methods described in Section 2, Fitting Procedure, we may write the following differential equation (Eq. 2.1)

$$\frac{d\boldsymbol{n}}{dt} = \boldsymbol{A}_{to}^{ad}\boldsymbol{n}$$

where $\boldsymbol{n}$ is vector of length 2. The first entry, n_1, is the probability that a myosin head is in the actin dependent role, has fluorescent ATP in its binding site and is unbound. The second entry, n_2, is the probability that a myosin head is in the actin dependent role, has fluorescent ATP in its binding site and is bound to actin (presumably myosin is weakly bound in this state). The matrix $\boldsymbol{A}_{to}^{ad}$ depends on the various rate constants, and, using the methods described in Section 2, we may write

$$\boldsymbol{A}_{to}^{ad} = \begin{bmatrix} -(k_n + k_a[A]) & k_d \\ k_a[A] & -(k_T + k_d) \end{bmatrix}$$

Still following the methods described in Section 2, we may solve this equation by determining the eigenvalues and eigenvectors of this matrix. Then, we may assemble these into a function made up of the sum of exponentials. Thus, for the actin-dependent heads we may write an expression for fluorescence (F_{ad}) as a function of time

$$F_{ad}(t) = A_1 e^{\lambda_1 t} + A_2 e^{\lambda_2 t}$$

where the exponential rates are the eigenvalues

$$\lambda_{1,2} = \frac{-(k_n + k_d + k_T + k_a[A]) \pm \sqrt{(k_T + k_d - k_n - k_a[A])^2 + 4k_d k_a[A]}}{2} \tag{6.1}$$

and the amplitudes may be determined from the eigenvectors and the initial condition vector. We assume that the initial condition vector $\boldsymbol{n}(0)$ can be written as

$$\boldsymbol{n}(0) = \begin{bmatrix} 1/2 \\ 0 \end{bmatrix}$$

that is, at the start of the experiment, half the heads are in the actin dependent role and have fluorescent ATP in their binding sites, and none of these heads are bound to myosin. With this assumption, the amplitudes are

$$A_{1,2} = \frac{1}{4} \pm \frac{k_T + k_d + k_a[A] - k_n}{4\sqrt{(k_T + k_d - k_a[A] - k_n)^2 + 4k_d k_a[A]}} \tag{6.2}$$

Similarly, for the non-/weak-binding heads, since actin turnover occurs at the rate k_n whether myosin is bound to actin or not, the rate constant matrix for non-binding heads, $\boldsymbol{A}_{to}^{nb}$, is

$$\boldsymbol{A}_{to}^{nb} = \begin{bmatrix} -(k_n + k_a[A]) & k_d + k_T \\ k_a[A] & -(k_n + k_d + k_T) \end{bmatrix}$$

So, the expression for fluorescence for the non-binding heads (F_{nb}) as a function of time is

$$F_{nb}(t) = A_3 e^{\lambda_3 t} + A_4 e^{\lambda_4 t}$$

where the exponential rates are the eigenvalues

$$\lambda_{3,4} = \frac{-(2k_n + k_d + k_T + k_a[A]) \pm (k_d + k_T + k_a[A])}{2}$$

And the amplitudes are

$$A_{3,4} = \frac{1}{4} \pm \frac{1}{4}$$

Since $A_4 = 0$, we have the particularly simple expression

$$F_{nb}(t) = \frac{1}{2} e^{-k_n t}$$

Thus, since the overall fluorescence (F) is the sum of the non-binding and actin-dependent fluorescence, the overall fluorescence is the sum of three exponentials

$$F(t) = A_1 e^{\lambda_1 t} + A_2 e^{\lambda_2 t} + \frac{1}{2} e^{-k_n t}$$

we can compare the predictions of this model with those of the full, optimized model by looking at these eigenvalues and amplitudes. We find excellent agreement (see Fig. 8), perhaps unsurprisingly, as the optimal switching rate is quite slow (see Table 1 in main text). However, both in the full model and in the calculations above, we find that the fluorescence decay is the sum of three (or more) exponentials. As these curves are well-fit by double exponentials (2–4), we must find a double-exponential approximation of this triple exponential.

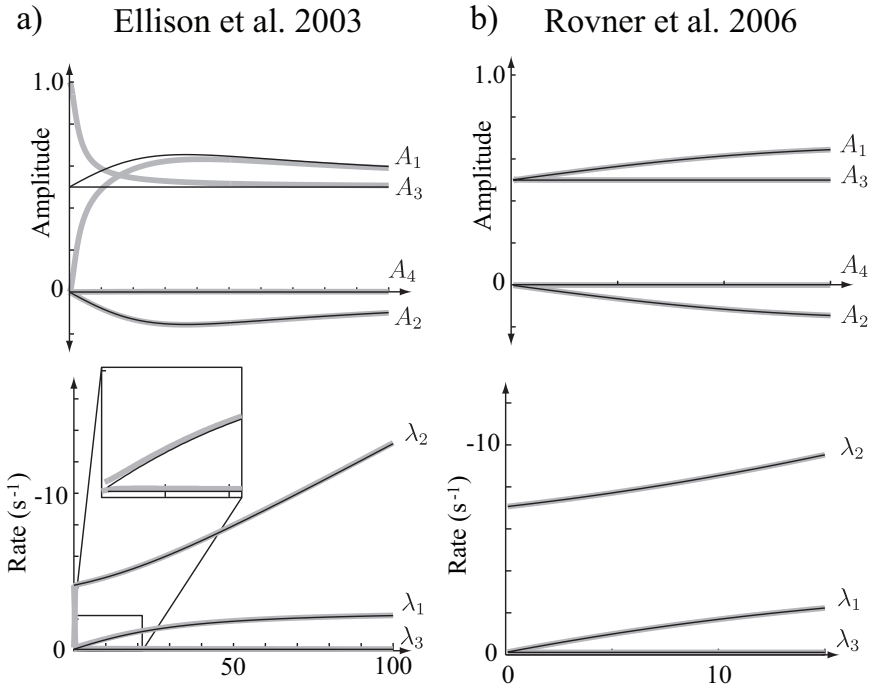

Figure 8: Amplitudes and rates for fluorescent decay. Amplitudes and rates from the exact solution (thick, gray lines) of the model with optimal parameters derived from a fit to the data of Ellison et al. (4) and Ellison et al. (2) in a, and from Rovner et al. (3) in b. Amplitudes and rates from the analytical fit model (thin, black lines), using the same parameters. The agreement is good. Note that there are three primary exponentials and that one has negative amplitude.

6.1.2 Fitting fluorescence decay with a double exponential

Here, we find an analytic expression for the rates and amplitudes of the double exponential fit to fluorescence decay. In order to do so, we assume that the amplitude and rate of the second exponential in the double exponential fit ($\mathcal{A}_2$ and ℓ_2, respectively) reflect the turnover rate of non-binding heads (e.g. $\mathcal{A}_2 = 0.5$ and $\ell_2 = -k_n$). Thus, we focus on the following problem: what exponential $\mathcal{A}_1 \exp(\ell_1 t)$ "optimally" fits the double exponential $A_1 e^{\lambda_1 t} + A_2 e^{\lambda_2 t}$? To answer this question, we must define precisely what defines an optimal fit.

Let us assume that we wish to minimize the mean squared error between the fluorescence decay curve $F(t) = A_1 e^{\lambda_1 t} + A_2 e^{\lambda_2 t} + 0.5 e^{-k_n t}$ and the double exponential fit $f(t) = \mathcal{A}_1 \exp(\ell_1 t) + 0.5 e^{-k_n t}$. Experimentally, the fluorescence is sampled at regularly occurring time points. Thus, we wish to minimize the

mean-squared difference (D) of the N measurements:

$$D \equiv \frac{1}{N}\sum_{i=1}^{N}(F(t_i) - f(t_i))^2$$

Since time is measured at regular intervals (Δt), and assuming we measure fluorescence over some time T, we may write $N = T/\Delta t$. Further, assuming that Δt is small, we may make a continuum approximation:

$$D = \frac{\Delta t}{T}\sum_{i=1}^{N}(F(t_i) - f(t_i))^2 \approx \frac{1}{T}\int_0^T (A_1 e^{\lambda_1 t} + A_2 e^{\lambda_2 t} - \mathcal{A}_1 \exp(\ell_1 t))^2 dt$$

We may reasonably assume that T is large, as most experimental measurements continue until fluorescence decays to its baseline value (3). Thus, in order to find the optimal fit, we must find the extrema of D as a function of $\mathcal{A}_1$ and ℓ_1:

$$\begin{aligned}\frac{\partial D}{\partial \mathcal{A}_1} &= \frac{1}{T}\left(-\frac{\mathcal{A}_1}{\ell_1} + \frac{2A_1}{\lambda_1+\ell_1} + \frac{2A_2}{\lambda_2+\ell_1}\right) = 0\\ \frac{\partial D}{\partial \ell_1} &= \frac{\mathcal{A}_1}{T}\left(\frac{\mathcal{A}_1}{2\ell_1^2} - \frac{2A_1}{(\lambda_1+\ell_1)^2} - \frac{2A_2}{(\lambda_2+\ell_1)^2}\right) = 0\end{aligned}$$

We can solve for $\mathcal{A}_1$:

$$\mathcal{A}_1 = \frac{2\ell_1 A_1(\lambda_2+\ell_1) + 2\ell_1 A_2(\lambda_1+\ell_1)}{(\lambda_1+\ell_1)(\lambda_2+\ell_1)} \tag{6.3}$$

Using this equation, we may obtain the following cubic equation for ℓ_1:

$$A_1(\lambda_2+\ell_1)^2(\lambda_1-\ell_1) + A_2(\lambda_1+\ell_1)^2(\lambda_2-\ell_1) = 0$$

which, being a cubic equation, can be solved analytically, providing an expression for the best-fit rate, ℓ_1, in terms of the amplitudes and rates that we may calculate using Eqs. 6.1 and 6.2. Then, we may use Eq. 6.3 to determine the best-fit amplitude, $\mathcal{A}_1$. These expressions constitute the analytical fit model.

Note that this model predicts that the faster, actin-dependent rate is the sum of two exponentials. One of these exponentials, the slower one, has an amplitude greater than 1/2, the other has a small, negative amplitude. Taken together, we predict that when we fit these curves with a single exponential, the best-fit amplitude should be greater than 1/2. As the fluorescence curve is fit with this single exponential plus the slower one (of amplitude 1/2 and rate $-k_n$), we predict that the faster exponential can have a larger amplitude than the slower one. Thus we may explain why the amplitude of the faster exponential in the best-fit to the data of Rovner et al. (3) is greater than 1/2, even though in Section 5 our simplified model predicts that the faster exponential has a maximum value of 1/2.

The analytical fit model avoids the numerical fit of a double exponential to the fluorescence decay in the full model, which increases simulation speed and optimization convergence. However, this speed comes at a cost: we must assume that $k_s \equiv 0$ and must make a continuum approximation for the fluorescence data. The optimum parameter values and their sensitivity ranges calculated with this method compare well to those calculated from the full optimization (see Fig. 9). Thus, we may be confident that our numerical optimization converged to the optimum value in the full model, and that our assumptions of negligible k_s and continuous fluorescence data are justified. However, the model is still quite complex.

6.2 The reduced model for 2P myosin

If we make a few simplifying assumptions motivated by the ATP turnover data of Rovner et al. (3) for expressed heavy meromyosin (HMM), we may derive an especially simple model, which we call the reduced model. This model allows us to understand parameter sensitivity and provides estimates for the parameters of the full model. We may then understand the results of the numerical optimization that, by themselves, provide little intuition about the system. Furthermore, as convergence is hard to demonstrate in numerical optimization, this simple model provides additional support to the conclusions of the full and analytical fit models.

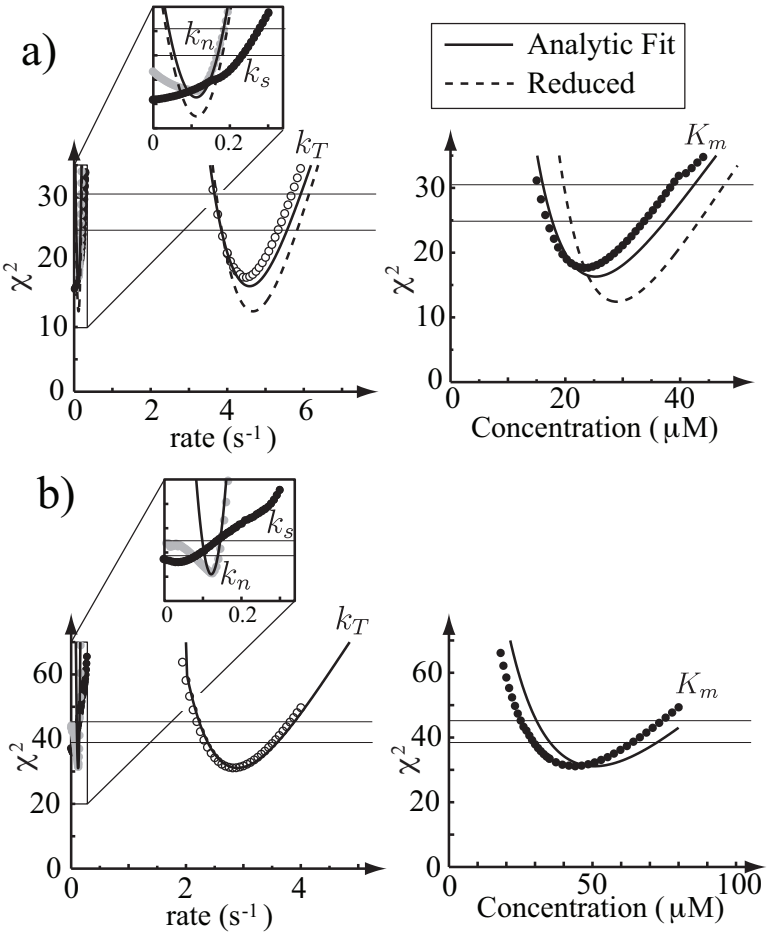

Figure 9: Parameter estimates and sensitivity analysis from the full model (dots) and the various approximations (analytic fit, solid black, reduced, dashed black). The analytic fit model provides an excellent estimate of optimum parameters and their error. The reduced model provides a good estimate. a) Fits from the steady-state and single turnover ATPase data of Rovner et al. (3). b) Fits from the data of Ellison et al. (4) and Ellison et al. (2). Note that we did not fit the reduced model to the data of Ellison et al. (4) and Ellison et al. (2), because the assumption of a linear single ATP turnover rate as a function of actin concentration does not apply.

Single ATP turnover from Rovner et al. (3) for both doubly (2P) and singly (1P) phosphorylated HMM were collected at low actin concentrations, such that the faster exponential rate for the fluorescence fit (ℓ_1) increases approximately linearly as the actin concentration increases. Based on this observation, we may perform expansions in $[A]/K_m$ for the exponential rates and amplitudes, where $K_m = (k_d + k_T)/k_a$. Keeping only first order terms (i.e. the linear terms) and assuming $k_T \gg k_n$, we may write

$$\begin{aligned} \lambda_1 &\approx -k_n - \frac{k_T[A]}{K_m} \\ A_1 &\approx \frac{1}{2} + \frac{k_T}{2(k_T + k_d)} \frac{[A]}{K_m} \end{aligned}$$

and

$$\begin{aligned}\lambda_2 &\approx -(k_T + k_d) - \frac{k_d[A]}{K_m} \\ A_2 &\approx -\frac{k_T}{2(k_T + k_d)} \frac{[A]}{K_m}\end{aligned}$$

Next, we make the simplifying assumption that $|A_2| << |A_1|$. This assumption is not quite correct, though at small actin concentrations it is reasonable (see Fig. 8). We then obtain the following relations:

$$\begin{aligned}\ell_1 \approx -k_n - \frac{k_T[A]}{K_m} \qquad & \mathcal{A}_1 \approx \frac{1}{2} \\ \ell_2 \approx -k_n \qquad & \mathcal{A}_2 \approx \frac{1}{2}\end{aligned}$$

The general equation for steady-state ATP turnover (Eq. 2.4) in the 2P model may be written simply as

$$V_{ATP} = k_n + \frac{k_n K_m + k_T[A]}{[A] + K_m} = k_n + \frac{k_n + k_T[A]/K_m}{[A]/K_m + 1}$$

which, assuming $k_T \gg k_n$ and that $[A]/K_m \sim O(1)$ (since the actin concentrations in the steady-state ATPase experiments were much larger than in the single ATP turnover experiments (3)), reduces to

$$V_{ATP} \approx \frac{k_T[A]}{[A] + K_m}$$

a Michaelis-Menten equation.

There are two important results from these equations. First, the simple model is a good approximation to the full model (see Fig. 10). Second, the simple model is specified by three parameters, k_n, k_T and K_m. The former result allows us to understand the relationship between the data and the parameters. The latter result allows us to understand parameter sensitivity.

From the reduced model, we see that the ATP turnover rate k_T is approximately equal to the maximal steady-state ATPase. We may estimate this value by fitting a Michaelis-Menten curve to these data. Rovner et al. (3) performed this fit and found $k_T \approx 4.8 \pm 0.6\text{s}^{-1}$. This value agrees well with the results of the full model, $k_T = 4.5 \pm 0.4\text{s}^{-1}$.

The reduced model predicts that the slower actin-independent exponential ℓ_2 should equal k_n. The single turnover data give $k_n = 0.11 \pm 0.034\text{s}^{-1}$ (average of data from Fig. 5b of (3)). This value agrees well with the results of the full model, $k_n = 0.11 \pm 0.04\text{s}^{-1}$.

Finally, the reduced model predicts two ways to estimate K_m. First, the Michaelis-Menten fit to the steady-state ATPase data, where Rovner et al. (3) report $K_m = 32 \pm 10\mu M$. Second, k_T divided by the slope of the actin-dependent rate ℓ_1, which is $(4.8 \pm 0.6\text{s}^{-1})/(0.15 \pm 0.05\text{s}^{-1}\mu M^{-1}) = 32 \pm 11\mu M$. In agreement with this value, the full model fits give $K_m = 23 \pm 5\mu M$. Thus, the reduced model allows us to easily estimate the various parameters (k_T, k_n and K_m), and provides a check to ensure that the numerical fits are reasonable.

The full model is fully specified by five parameters, k_n, k_T, k_s, k_d and k_a. However, the reduced model has three parameters, k_n, k_T and K_m, and assumes that $k_s = 0$. Thus, since the reduced model fits the data of Rovner et al. (3) reasonably well, we expect the full model to be relatively insensitive to k_a and k_d, depending rather on $K_m = (k_T + k_d)/k_a$. Indeed, we find that the full model is so insensitive to these parameters, that they may vary over several orders of magnitude (e.g. fixing $k_d = 1 \cdot 10^6\text{s}^{-1}$ or $k_d = 0.01\text{s}^{-1}$ both generate curves that fit the data). Conversely, the full model gives well-defined estimates for each of the reduced parameters.

6.3 The analytical fit model for 1P myosin

The model for HMM-1P is more complex than that of HMM-2P, so that simply assuming small k_s does not result in analytic results. Thus, in order to circumvent the numerical double-exponential fits in the HMM-1P

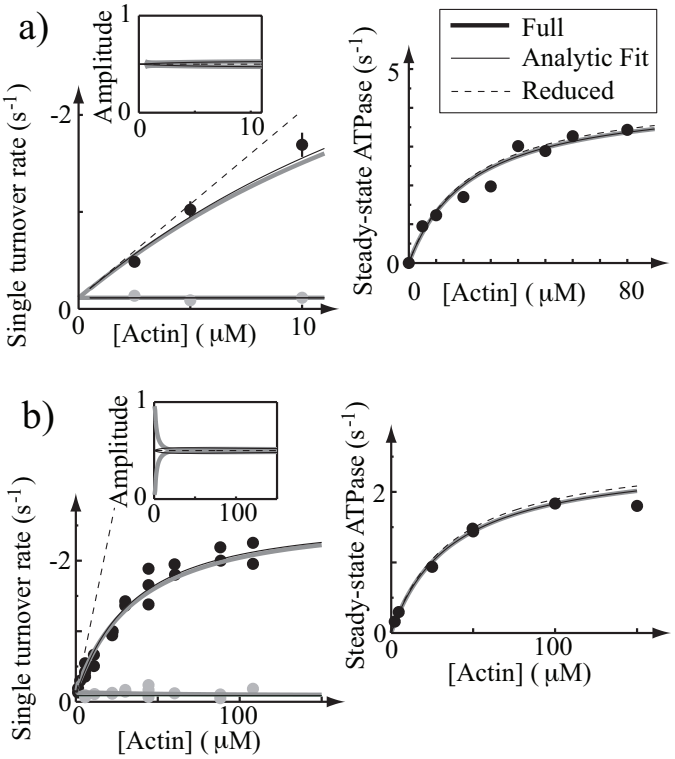

Figure 10: Approximations to the full model. The full model (thick line), the analytic fit model (thin line) and the reduced model (dashed line) are shown, along with data. The same parameters are used for all simulations. The analytic fit model is an excellent approximation of the full model. For the single ATP turnover experiments, the reduced model is a good approximation at small actin concentrations. a) For the data of Rovner et al. (3), the reduced model is an adequate approximation. b) For the single turnover ATP turnover data of Ellison et al. (4), the reduced model is a poor approximation, as actin concentrations are not small.

model, we must make an additional assumption. We assume that the equilibrium between the folded and extended conformations occurs very rapidly compared to the other rates. Note that there is no apparent reason for this assumption to be true, we therefore justify it by the fact that it leads to a simple model, and the fact that that model fits the data as well as the full model.

Making the rapid equilibrium assumption, the probability of being in the unfolded state while detached (a_1) is

$$a_1 = \frac{1}{1 + k_2/k_3}$$

Similarly, the probability of being in the unfolded state while weakly bound (a_2) is

$$a_2 = \frac{1}{1 + k_2'/k_3'}$$

These expressions allow us to write an equivalent attachment rate, k_a^{eff}, the probability of being in the unfolded conformation times its attachment rate plus the probability of being in the folded conformation times its attachment rate:

$$k_a^{eff} = a_1 k_a + (1 - a_1) k_a^*$$

similarly, the effective detachment rate, k_d^{eff} is

$$k_d^{eff} = a_2 k_d + (1 - a_2) k_d^*$$

With these expressions, we may use precisely the same methods as for the 2P analytic-fit model to derive a 1P analytic-fit model. Additionally, when we evaluate the general equation for steady-state ATP turnover (Eq. 2.4) in the 1P model, we find

$$V_{ATP}^{1P} = \frac{2a_1 k_n K_m^{1P} + a_2(k_T + k_n)[A]}{K_m^{1P} + [A]}$$

where $K_m^{1P} = (a_2 k_T + k_d^{eff})/k_a^{eff}$. This model fits the data well (not shown), and the optimum parameter values and their sensitivity ranges calculated with this method compare well to those calculated from the full optimization (see Fig. 11). Thus, we may be confident that our numerical optimization converged to the optimum value in the full model, and that our assumptions of negligible k_s and continuous fluorescence data are justified.

6.4 The reduced model for 1P myosin

Here we derive a very simplified version of the 1P myosin model that we call the reduced model. As with the 2P reduced model, we may use the reduced HMM-1P model to understand results of the numerical optimization and to support the conclusions of the full and analytical models.

Following the derivation of the reduced 2P model, we get

$$\ell_1^{1P} \approx -a_1 k_n - \frac{a_2 k_T [A]}{K_m^{1P}} \qquad \mathcal{A}_1^{1P} \approx \frac{1}{2}$$

$$\ell_2^{1P} \approx -\frac{a_1 + a_2}{2} k_n \qquad \mathcal{A}_1^{2P} \approx \frac{1}{2}$$

and

$$V_{ATP}^{1P} \approx \frac{a_2 k_T [A]}{K_m^{1P} + [A]}$$

a Michaelis-Menten equation.

These equations are a good approximation of the full model (see Fig. 11). Together, this model and the 2P reduced model are specified by 6 parameters: a_1, a_2, K_m^{1P}, k_T, k_n and K_m. As with the 2P reduced model, these results will allow us to understand the relationship between the data and the parameters, and to understand parameter sensitivity.

The ATP turnover rate is approximately equal to the maximal steady-state ATPase rate. In the 2P reduced model, we found this value to be k_T. In the 1P reduced model, it is $a_2 k_T$. Thus the ratio of these maximal rates, V_{max}^{1P}/V_{max} should be a_2. Rovner et al. (3) measured these values, and found $V_{max}^{1P}/V_{max} = 3.1 \pm 0.4/4.8 \pm 0.6 = 0.65 \pm 0.12$. Numerical optimization of the full model found $a_2 = 0.71 \pm 0.14$, in agreement with this value.

We may estimate a_1 either through the slower actin-independent rate ℓ_2^{1P} or through the faster actin-dependent rate ℓ_1^{1P}. Since the slower actin-independent rate has a large error, perhaps the best estimate of a_1 is the ratio of the y-intercepts of the actin-dependent rates as a function of actin: $\lim_{[A]\to 0} \ell_1^{1P} = -a_1 k_n = -0.084 \pm 0.09 \mathrm{s}^{-1}$. As $k_n = 0.11 \pm 0.04 \mathrm{s}^{-1}$ from the 2P reduced model, we predict $a_1 = 0.76 \pm 0.86$, in reasonable agreement with the results from numerical optimization. Note that we expect this parameter to be variable, since even the more accurate estimation method is uncertain.

As with the 2P reduced model, there are two ways to estimate K_m^{1P}, the Michaelis-Menten fit to steady-state ATPase, and $a_2 k_T$ divided by the slope of the actin-dependent rate, ℓ_1. Rovner et al. (3) report a $K_m^{1P} = 26 \pm 9 \mu M$. The second method gives $3.1 \pm 0.4/0.10 \pm 0.02 \mu M = 31 \pm 7 \mu M$. Both of these estimates agree with the result from numerical optimization: $K_m^{1P} = 26 \pm 9 \mu M$.

The full 1P model is fully specified by eleven parameters, k_2, k_3, k_2', k_3', k_d^*, k_a^*, k_n, k_T, k_s, k_d and k_a. There is, additionally, the constraint that mass/energy must be conserved, so we have 10 free parameters. However, the reduced model has six parameters, a_1, a_2, K_m^{1P}, k_n, k_T and K_m, and assumes that $k_s = 0$. Thus, since the reduced model fits the data of Rovner et al. (3) reasonably well, we expect the full model to be relatively insensitive to k_2, k_3, k_2', k_3', k_a^*, k_d^*, k_a and k_d, depending rather on $a_1 = 1/(1 + k_2/k_3)$, $a_2 = 1/(1 + k_2'/k_3')$, $K_m^{1P} = (a_2 k_T + a_2 k_d + (1 - a_2)k_d^*)/(a_1 k_a + (1 - a_1)k_a^*)$ and $K_m = (k_T + k_d)/k_a$. Again, the full model gives well-defined estimates for each of the reduced parameters while the individual parameters are variable.

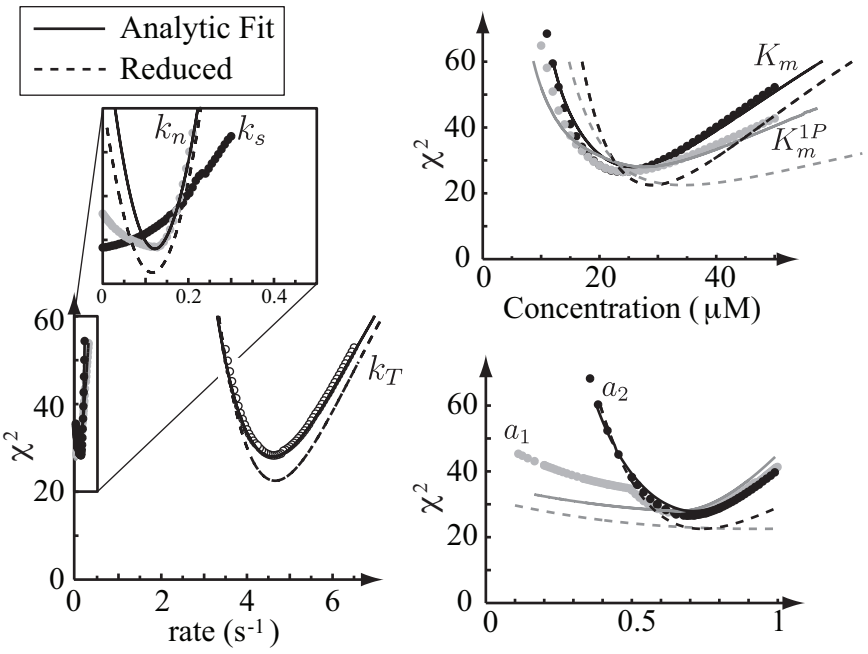

Figure 11: Parameter estimates and sensitivity analysis from the full 1P and 2P myosin model (dots) and the various approximations (analytic fit, solid black, reduced, dashed black). The analytic fit model provides an excellent estimate of the optimum parameters and their error. The reduced model provides a good estimate. The data are from Rovner et al. (3).

7 Asymmetric model, an alternate model for 1P myosin

We might not expect a phosphorylated head to behave identically to an unphosphorylated head. In particular, since unphosphorylated myosin is thought to be more flexible than phosphorylated (7), we might expect that, say, if the unphosphorylated head is in the weak-binding role, it might form the inhibited complex. Alternatively, when it is in the strong-binding role, the molecule would not have the freedom to adopt the inhibited state. The model is shown in Fig. 12a. We refer to this model as the "asymmetric" model, due to the asymmetric appearance of the kinetic scheme, as opposed to the symmetric appearance of the kinetic scheme when either head may form the inactive, folded conformation with equal probability. We therefore refer to this latter model the "symmetric" model.

The best-fit parameters for this model were determined with optimization. The fit is shown in Fig. 12b. Like the symmetric model, the asymmetric model fits the data well ($p < 0.05$). Thus, we conclude that this model is consistent with the data.

Note that both the symmetric and asymmetric models predict that activity in smooth muscle is modulated by a phosphorylation-dependent equilibrium between the inactive, folded conformation and the extended, active conformation. The symmetric model, however, assumes that this equilibrium is independent of the role (e.g. weak-/non-binding or actin-dependent) of the phosphorylated head; while the asymmetric model assumes that the equilibrium only occurs when the phosphorylated head assumes one of those roles. Functionally, it would therefore appear in some assays that, in the symmetric model, singly phosphorylated (1P) myosin is a uniform population of partially active molecules. Alternatively, in the asymmetric model, since role switching is slow, 1P myosin would appear to be a non-uniform population of fully active and mostly inactive molecules. In a recent paper, we concluded that our mechanical data for single phosphorylated myosin were consistent with exactly these two mechanisms: a uniform population of partly active, or a non-uniform population of active and inactive molecules (8). Here, in addition to showing that the two heads of myosin adopt non-equivalent roles over long time scales, we have provided mathematical detail to this statement, and show that these detailed mathematical models are consistent with biochemical data. Further, based on

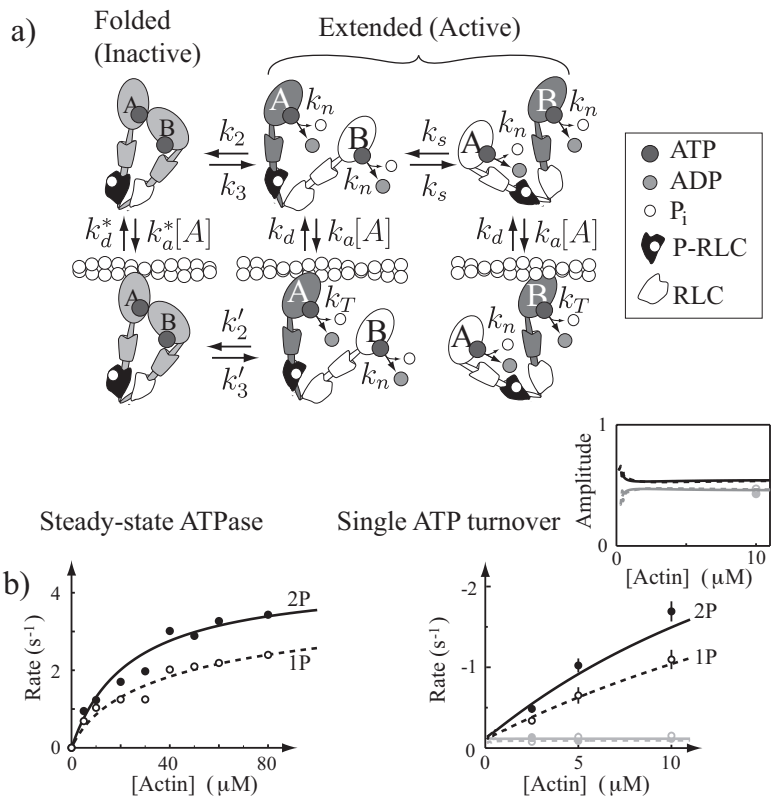

Figure 12: The asymmetric model fits the data of Rovner et al. (3) for 2P and 1P myosin. a) A sketch of the model. The molecule forms the folded (inactive) conformation only when the phosphorylated head assumes the actin-binding role. Thus, since role switching is slow, 1P myosin is either partially active (if the phosphorylated head assumes the actin-binding role) or fully active (if the phosphorylated head assumes the non-/weak-binding role). b) Like the symmetric model, where 1P myosin may form the folded state irrespective of the role of the phosphorylated head, the asymmetric model fits ($p > 0.5$) the single ATP turnover and steady-state ATPase data of Rovner et al. (3).

the detail, we may design experiments to distinguish the two.

References

1. Walcott, S., and W. Herzog, 2008. Modeling residual force enhancement with generic cross-bridge models. *Mathematical Biosciences* 216:172–186.

2. Ellison, P. A., Z. S. DePew, and C. R. Cremo, 2003. Both heads of tissue-derive smooth muscle heavy meromyosin bind to actin in the presence of ADP. *Journal of Biological Chemistry* 278:4410–4415.

3. Rovner, A. S., P. M. Fagnant, and K. M. Trybus, 2006. Phosphorylation of a single head of smooth muscle myosin activates the whole molecule. *Biochemistry* 45:5280–5289.

4. Ellison, P. J. R. Sellers, and C. R. Cremo, 2000. Kinetics of smooth muscle heavy meromyosin with one thiphosphorylated head. *Journal of Biological Chemistry* 275:15142–15151.

5. Veigel, C., J. E. Molloy, S. Schmitz, and J. Kendrick-Jones, 2003. Load-dependent kinetics of force production by smooth muscle myosin measured with optical tweezers. *Nature Cell Biology* 5:980–986.

6. Kad, N. M., J. B. Patlack, P. M. Fagnant, K. M. Trybus, and D. M. Warshaw, 2007. Mutation of a conserved glycine in the SH1-SH-2 helix affects the load-dependent kinetics of myosin. *Biophysical Journal* 92:1623–1631.

7. Tama, F., M. Feig, J. Liu, C. L. Brooks III, and K. A. Taylor, 2005. The requirement for mechanical coupling between head and S2 domains in smooth muscle myosin ATPase regulation and its implications for dimeric motor function. *Journal of Molecular Biology* 345:837–854.

8. Walcott, S., P. M. Fagnant, K. M. Trybus, and D. M. Warshaw, 2009. Smooth muscle heavy meromyosin phosphorylated on one of its two heads supports force and motion. *Journal of Biological Chemistry* 284:18244–18251.